Oscillations of a chemical garden

J. Pantaleone,[1] A. Toth,[2] D. Horvath,[2] J. Rother McMahan,[3] R. Smith,[3] D. Butki,[3] J. Braden,[3] E. Mathews,[3] H. Geri,[3] and J. Maselko[3]

[1]*Department of Physics, University of Alaska, Anchorage, Alaska 99508, USA*

[2]*Department of Chemistry, University of Szeged, Szeged, Hungary*

[3]*Department of Chemistry, University of Alaska, Anchorage, Alaska 99508, USA*

(Received 24 November 2007; published 11 April 2008)

When soluble metal salts are placed in a silicate solution, chemical gardens grow. These gardens are treelike structures formed of long, thin, hollow tubes. Here we study one particular case: a calcium nitrate pellet in a solution of sodium trisilicate. We observe that tube growth results from a relaxation oscillation. The average period and the average growth rate are approximately constant for most of the structures growth. The period does fluctuate from cycle to cycle, with the oscillation amplitude proportional to the period. Based on our observations, we develop a model of the relaxation oscillations which calculates the average oscillation period and the average tube radius in terms of fundamental membrane parameters. We also propose a model for the average tube growth rate. Predictions are made for future experiments.

DOI: 10.1103/PhysRevE.77.046207 PACS number(s): 89.75.Kd, 82.40.Bj

I. INTRODUCTION

When soluble metal salts are placed in solutions containing silicates, they grow treelike structures built from hollow tubes. These structures are known by many names: chemical gardens, crystal gardens, silica or silicate gardens, or colloidal gardens. The first know observation of these structures was several centuries ago by Glauber [1]. Because of their resemblance to biological organisms, these systems were investigated a century ago by scientists interested in the origin of life [2]. These days, chemical gardens are studied for a variety of reasons. The formation of Portland cement can be viewed as a type of silicate-garden system where calcium silicates placed in water form a mesh of thin calcium silicate hydrate tubes [3]. More popularly, chemical gardens are a common activity for science education (see, e.g., [4]) and have even been grown aboard the space shuttle [5].

The different chemical garden systems have in common many qualitative features [6]. When the metal salt is placed in the silicate solution, it begins to dissolve and at the same time a semipermeable membrane forms around it. Water is driven across the membrane and into the structure by osmosis, further dissolving the metal salt. This intake of water also increases the internal physical pressure, which somehow causes the structure to grow. The mechanism behind how a structure grows depends on the type of metal salt and the concentration of the silicate solution. Some systems are observed to grow vertical tubes driven by a large bubble at the top of the tube (see, e.g., [7]). Other systems are observed to grow long, continuous tubes which are open at the end (see, e.g., [8]). It has also been proposed that some systems develop fingers from a generic Laplacian instability [9]. In addition, it has been observed since the early days that some tubes appear to be segmented [2,10] and so must result from a periodic growth mechanism. Thus within the family of chemical garden systems, the details of the growth mechanism vary widely. Most studies of these systems have focused on the relevant chemistry and the associated morphology while the physical details of the growth mechanism have generally not been explored.

The chemical garden we focus on in this paper grows via an oscillatory growth mechanism. When the internal pressure gets large enough, the membrane ruptures, internal solution emerges, and new membrane quickly forms on the exposed interface, sealing the rupture. This pattern repeats itself to form long, twisting tubes. Similar behavior has been observed in experiments that directly pump metal salt solution into silica solution [11–13]. The general mechanism is somewhat similar to the cyclic eruptions of volcanic domes (see, e.g., [14] and references therein).

A unique property of our system is that the entire structure is observed to "bow" or "twitch" periodically as the structure grows. We have videotaped this motion and analyzed the recordings to gain insight into the growth mechanism. In Sec. II we describe our experimental procedure. In Sec. III we present our experimental results. In Sec. IV we discuss the implications of our observations and propose some models to explain the oscillations and the tube growth. In Sec. V we summarize our results and propose future experiments that would help determine some of the important details of the growth mechanism.

II. EXPERIMENTAL PROCEDURE

Our experiment involves placing a 1.0-g pellet of ground calcium nitrate crystal into 250 ml of aqueous sodium trisilicate solution. The calcium nitrate was ground using an IKA basic grinder for 15 s to create a fine powder, which we then weighed and pressed using an International Crystal Laboratories compressor. The 250 ml of solution was composed of 5 ml hydrochloric acid (0.6 M) and 245 ml sodium trisilicate (1.0 M, Sigma Aldrich). This solution was placed in a rectangular plastic container which resulted in a column height of 8.5 cm. The calcium nitrate pellet was then placed near the center of the solution and dropped to the bottom of the container. The experiments were performed at 20 ± 1 °C.

A digital video camera was used to monitor the growth and the oscillatory behavior of the silica tubes. A digital image processing program was used to evaluate the video frame

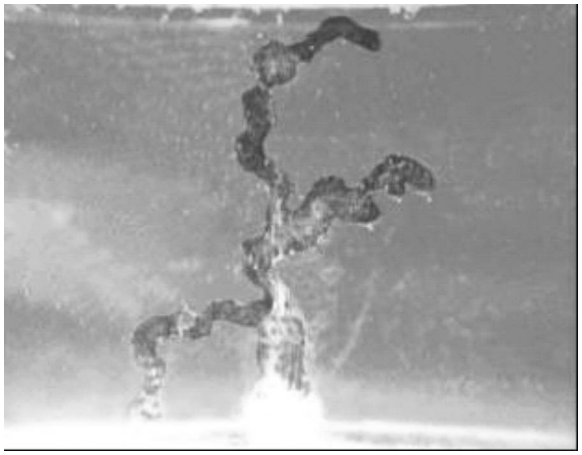

FIG. 1. Photograph of typical structure observed in our experiment. The diameter of the base stem is 1.0 cm.

by frame (each frame was 780 pixels by 420 pixels) in gray scale at 30 frames per second capture rate. The movement of the tube was monitored by taking advantage of the contrast between the light colored tube wall and the darker background. The point of inflection was located along a vertical or horizontal line of subsequent frames, depending on the orientation of the tube. We constructed a time series using this inflection point for each clip of video that we found oscillations or clear growth.

III. EXPERIMENTAL RESULTS

An example of the structures observed in our experiment is shown in Fig. 1. Note that the structure has vertical and horizontal segments. Most experiments on chemical gardens are conducted in the regime where the density of the inner solution is substantially smaller than that of the outer solution. Then the buoyant force results in vertical structures. However, in our case the density difference between the inner and outer solutions must be relatively small to allow the formation of horizontal structures as well. We observed that tubes generally grow vertically when they first emerge from the base, but eventually they curve over and start growing horizontally.

When the pellet is first placed in the liquid, a membrane forms over the surface of the pellet. Osmosis drives fluid into the structure, dissolving the calcium nitrate and increasing the internal pressure. After about 15 min, a point on the membrane ruptures and a tube starts to grow. Figure 2 shows

FIG. 2. Sequence of images showing the growth of a tube (field of view: 2.1 cm $\times$ 2.0 cm).

FIG. 3. Bowing chemical system. The picture shows the superposition of two pictures taken 2 s apart. This indicates the range of motion of the structure over the course of a single "bow."

a sequence of images illustrating the horizontal growth of a tube. Note the twisting nature of the tube growth. This occurs because the tube grows by a series of ruptures near the tip. After the first tube grows for a while it can stop growing (sometimes because it hits a wall or the floor) and then another tube starts growing from somewhere near the base. As shown in Fig. 1, multiple tubes are common. The base is typically about a centimeter across, while the tubes are about 1–2 mm in diameter. Each tube can grow to be several centimeters long. About 60–90 min after it began, tube growth stops.

An amazing property of tube growth is that the entire structure is observed to move regularly. Figure 3 illustrates this motion by superimposing two pictures taken 2 s apart. The horizontal segments are observed, over a second or two, to gradually bow. This bowing motion is subsequently undone in one quick motion. For most of our observations, the slow motion is downward and the quick motion is upward. Figure 4 shows the change in position over time for one

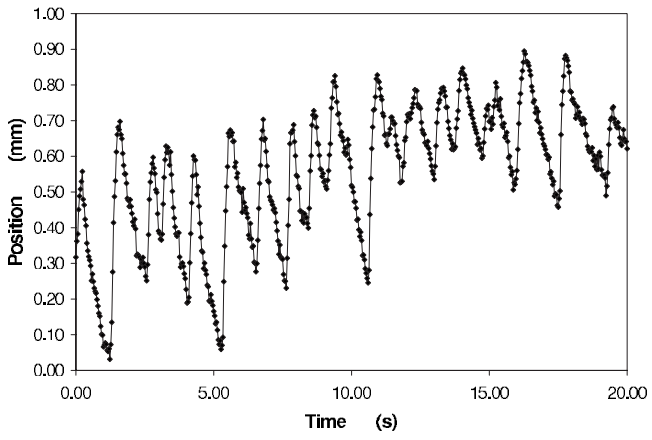

FIG. 4. Position versus time for vertical motion of a tube. The sawtooth pattern is a clear indication of a relaxation oscillation. The time $t=0$ corresponds to 104 min after the pellet was dropped into the silicate solution.

particular point on the structure. The observed sawtooth pattern is characteristic of a relaxation oscillation.

The driving force for the movement is osmosis. Osmotic pressure causes water to flow into the membrane, slowly increasing the internal pressure. As the internal pressure builds up, the membrane bows. Eventually the membrane ruptures, quickly releasing the pressure and allowing the structure to return to its relaxed state. When the membrane ruptures, internal calcium nitrate solution emerges through the rupture into the sodium silicate solution. New membrane quickly forms around the emitted solution, enlarging the system. The processes involved in this relaxation oscillation are shown in Fig. 5. Note that Fig. 4 only shows a small part of the growth of one tube. Typically it takes several hundred oscillations to grow an entire tube.

Position versus time data similar to those in Fig. 4 were taken over much longer time intervals for the growth of several different tubes. These data were analyzed to extract the time of each quick motion and the associated change in position of the reference point during the quick motion. The resulting data were then analyzed in several different ways.

The time interval between the quick jumps in tube position is the period of the relaxation oscillation. This period fluctuates from cycle to cycle. Figure 6 shows the distribution of the oscillation periods. The figure plots the number of periods greater than T versus T. The data are all from one continuous observation of the growth of a single tube. Note that the plot is relatively constant at short time intervals, indicating that there are few short time intervals. This result is robust, insensitive to the procedure used to identify the quick jumps. At longer time intervals, the log-linear plot shows that the distribution decreases exponentially with T. This is similar to the behavior observed in rock fractures [15], where the fractures are described as stochastic. To examine correlations in our data, we show a time delay plot in Fig. 7 and two autocorrelation plots in Fig. 8. Figure 7 plots one time interval versus the preceding time interval, and the data here appear to show stochastic fluctuations around an average value. Figure 8 shows the autocorrelation of two other pieces of the data. For both data sets the $n>1$ correlations are small and consistent with stochastic fluctuations around an average value. However, at $n=1$ the two analyses

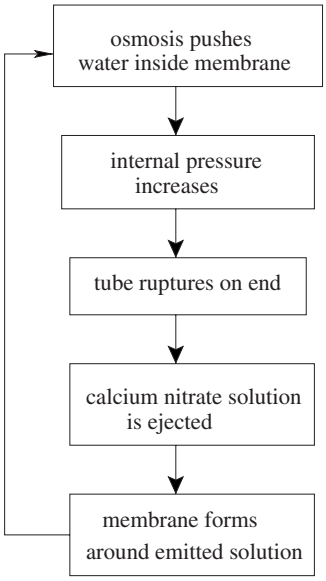

FIG. 5. Flow chart for the relaxation oscillation.

both give essentially the same value, 0.24, which may be significant. An interpretation of this is given in Sec. IV D. In general, the data indicate that the rupture process has a stochastic component that varies from one rupture to the next.

Figure 9 shows the amplitude of the quick motion versus the period *preceding* the quick motion for two pieces of the data. It is apparent that their is a strong correlation between the amplitude and the preceding period. In general, the longer the time interval over which the pressure builds up, the larger the amplitude of the quick motion when that pressure is released. These results are completely consistent with the relaxation oscillation process described here. We note that for the observed motion at other times, the correlation was generally smaller but still significant.

Figure 10 shows how the period of the oscillations changes over long times. Each data point is the average over 20 oscillations. The data indicate that the average period is relatively constant, with an increase in time at late times.

The videotapes of the structure were also analyzed to give the rate of tube growth. Length information is difficult to

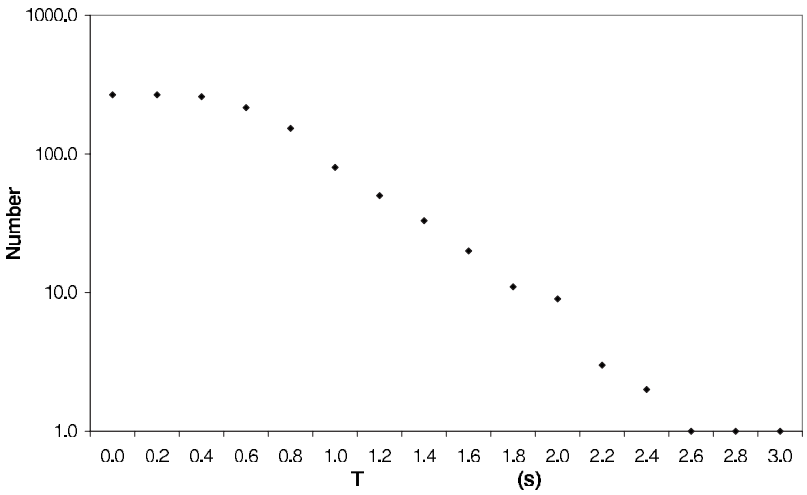

FIG. 6. Distribution of periods observed during the growth of one tube. Plot of number of intervals greater than T versus T. Data are for 101–105 min after pellet was dropped into the silicate solution.

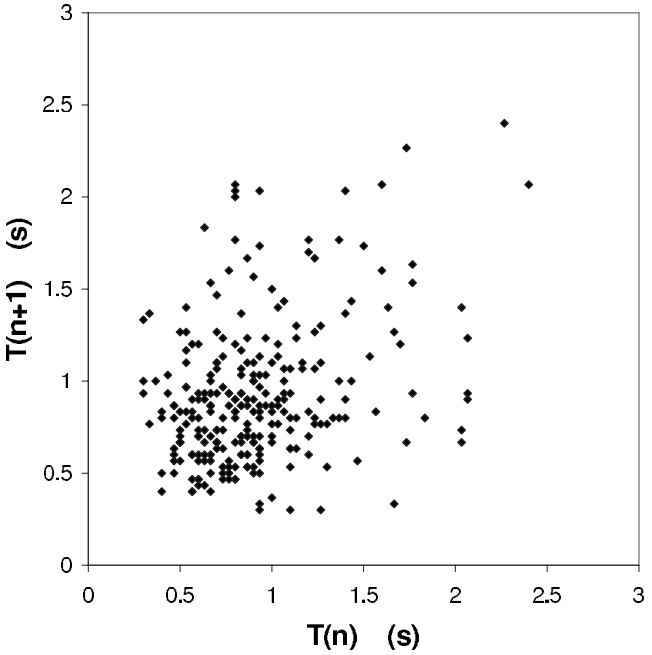

FIG. 7. Distribution of time intervals for the growth of one tube. Plot of one time interval versus the preceding time interval. Data are for 101–105 min after pellet was dropped into the silicate solution.

reliably extract when the tubes grow in a twisting fashion. However, when each tube first starts to grow from the base, they generally grow straight upwards for a short period of time. Figure 11 shows the initial length increase for three tubes which grew from the same base. The observed growth rates were 0.22 mm/s for the start of tube 1 (circles), 0.24 mm/s for the start of tube 2 (squares), and 0.21 mm/s for the start of tube 3 (diamonds). Note that the vertical offset between the data sets is arbitrary since it is not possible to accurately measure the total tube length after the initial straight growth.

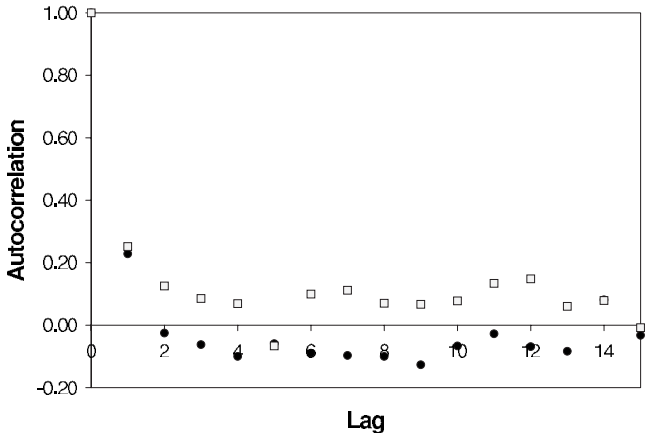

FIG. 8. Autocorrelation of the data versus the lag. The solid circles (open boxes) correspond to data from the 35th and 36th (48th and 49th) minutes after the pellet was dropped into the silicate solution.

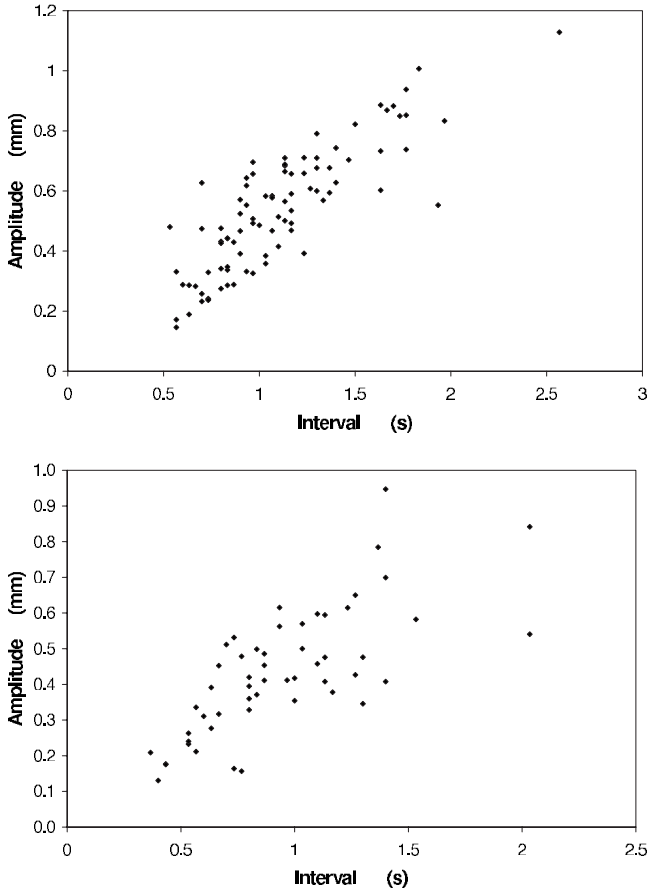

FIG. 9. Amplitude of quick motion versus preceding time interval (in seconds). The longer the time interval, the longer the internal pressure has to build up, the larger the pressure released at rupture. The top (bottom) graph corresponds to data from the 49th (104th) minute after the pellet was dropped into the silicate solution.

IV. INTERPRETATION OF RESULTS

A. Membrane stresses

Tubes grow because the membrane ruptures consistently at or near the end of the tube. Membranes rupture when they reach a critical value of the stress, σ_c. To understand the implications of this we shall examine the stresses in the approximately hemispherical base and in the long, thin tubes [16].

For a spherical pressure vessel with an internal pressure that is P higher than the outside, the upward force on the top half of the membrane is $\pi R^2 P$ where R is the radius of the sphere. This force is distributed along the edge of the membrane so that the stress in the membrane is the total force over the cross-sectional area of the membrane:

$$\sigma_{sphere} = \frac{\pi R^2 P}{2\pi R \tau} = \frac{PR}{2\tau}. \tag{1}$$

Here τ is the thickness of the membrane. Because of the symmetry of a spherical surface, the stress is the same in any direction. However, for a tube, the stresses are different in different directions. Proceeding similarly to the calculation

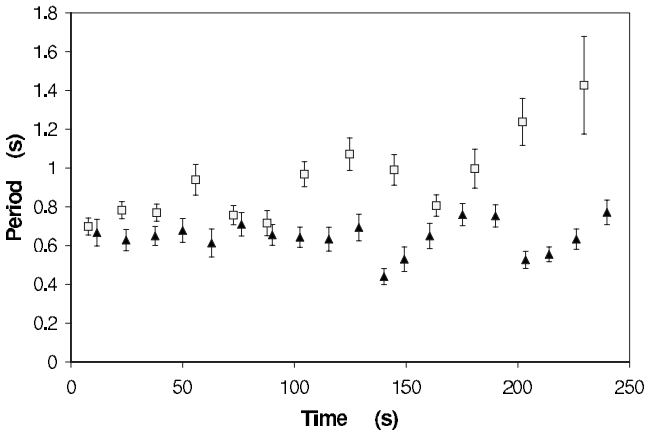

FIG. 10. Average period of the relaxation oscillation versus time. The intervals between the quick motion are averaged over 20 cycles, and the error bars indicate the standard deviation of these 20 cycles. For the solid triangles (open boxes) $t=0$ corresponds to 35 (101) min after the pellet was dropped into the silicate solution.

above, the longitudinal and transverse stresses in a long, closed cylinder are

$$\sigma_{longitudinal} = \frac{PR}{2\tau},$$

$$\sigma_{transverse} = \frac{PR}{\tau}, \tag{2}$$

where R is now the radius of the tube. The internal pressure produces these stresses in the membrane.

These calculations can only serve as an approximate guide to the stresses in the membrane since the system is actually not uniform or symmetric. The tube grows with many changes in direction and the base often has several tubes emerging from it. The asymmetry and nonuniformities in the geometry of the membrane give rise to corresponding differences in the stresses and so also in the strains. Thus as the pressure in the system changes, the membrane will stretch somewhat differently at different locations. These nonuniform strains will cause the system to "flex" and/or move slightly. The above stress formulas indicate that the stresses are generally larger in the base than along the tube; thus, it is reasonable to expect that the strains are larger there too. Nonuniform strains in the base would cause the tubes to move as a whole as is generally observed. This is probably the leading factor in what produces the observed motion of the system during the pressure cycles. However, there is another possible contribution to the motion. As the pressure changes, the size of any small air bubbles that might be trapped in the structure will change also, causing a change in the buoyant force on the structure. Future experiments are needed to sort out the relative importance of these two possible contributions to the motion of the structure.

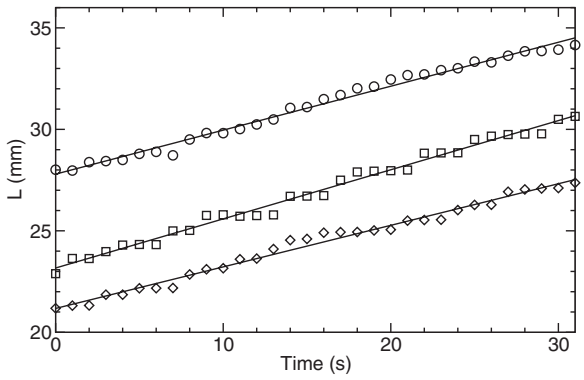

FIG. 11. The increase in tube length for the initial growth of three different tubes emerging from the same base. The circles are for the start of tube 1, the squares are for the start of tube 2 (16 min later), and the diamonds are for the start of tube 3 (31 min after tube 1 starts). The vertical offset between the different data sets is arbitrary.

Now let us use these stress equations to try and understand the rupture process. Note that in a tube, the transverse stress is larger by a factor of 2 than the longitudinal stress. This is why when hot dogs are cooked they tend to split along the longitudinal axis. Because the tube does not rupture longitudinally, but at the end, this implies that the membrane must be more fragile there. This conclusion is reinforced by comparing the stresses in the base to those at the end of the tube. Treating the end of the tube as a hemisphere, the radius of curvature there is much smaller than that of the base, so the stresses should be considerably less at the end of the tube. The fact that the membrane ruptures consistently at the end of the tube tells us again that the membrane must be much more fragile there. Assuming the membrane material is uniform and interpreting this in terms of thickness differences gives approximately

$$\frac{\tau_{tube\ end}}{\tau_{base}} < \frac{R_{base}}{R_{tube\ end}} \approx 5 - 10. \tag{3}$$

Therefore, the membrane of the tube-base system must be much thinner and/or fragile at the end.

The tube end is special because it is the youngest membrane on the structure. Equation (3) implies that the membrane at the tube end is far from its final-state thickness and strength when the rupture occurs. However, note that, as seen in Fig. 4, the bowing starts immediately after the relaxation to the unbowed state. This indicates that a membrane has formed and is capable of supporting pressure at the earliest observed times after rupture. The data imply that new membrane grows very quickly at first, but that the time scale for reaching its final state thickness and strength is much longer than the typical oscillation period.

B. Pressure and the oscillation period

The relaxation oscillation is driven by the flow of water through the membrane and into the system from osmosis. This flow causes the internal pressure of the system to increase. To understand how the system responds to the pressure increase, we consider a crude model of the system as a composite pressure vessel made of an approximately hemispherical base and a tube(s).

A pressure increase ΔP in response to the volume inflow ΔV is usually written as

$$\Delta P = B\frac{\Delta V}{V}, \tag{4}$$

where B is the bulk modulus. For a composite pressure vessel made of a hemispherical base and a tube(s), Eq. (4) can be rewritten as

$$\Delta P = \frac{B_T B_B}{B_B V_T + B_T V_B}\Delta V, \tag{5}$$

where the subscripts T and B denote quantities corresponding to the tube and the base, respectively. The bulk moduli can be calculated under the simplifying assumptions that the membrane is uniform everywhere and that it responds elastically. Although our previous discussion of stresses in the membrane indicated that the tube end must be different than the rest of the tube, the tube end was not observed to visible expand while the pressure was building up. The tube end is a relatively small area, and we will neglect it in the calculation of a global quantity. Then

$$B_B = \frac{2}{3}\left[\frac{1}{1-\nu}\right]\frac{E}{R_B}\tau \tag{6}$$

and

$$B_T = \left[\frac{2}{5-3\nu}\right]\frac{E}{R_T}\tau, \tag{7}$$

where E is Young's modulus and ν is Poisson's ratio. Taking $\nu \approx 0.5$ (the value for a perfectly incompressible material that deforms elastically) and using the expression for the volumes, the pressure-volume relation for the system is approximately

$$\Delta P \approx \frac{E\tau}{5.5R_T^3 L + 1.6R_B^4}\Delta V, \tag{8}$$

where L is the total length of all the tubes in the system. This equation shows that the small radius of the tube greatly suppresses the tube's contribution to the pressure-volume relationship. Given the observed ratio of radii [see Eq. (3)], it is reasonable to neglect the contribution of the tube(s) to the pressure-volume relationship.

As water flows into the system, the pressure increases until it reaches a critical pressure P_c and rupture occurs. The period of the relaxation oscillation, T, is approximately just the time for this slow process; i.e., the time for the pressure release can be neglected. Using Eq. (8), with the contribution of the tube neglected, we have

$$T \approx P_c\left[\frac{1.6R_B^4}{E\tau}\right]\frac{1}{dV/dt}, \tag{9}$$

where dV/dt is the flow rate of fluid into the structure from osmosis. Now dV/dt would be difficult to measure directly, but it can be related to other observables. The fluid that flows into the structure causes the structure to grow, so dV/dt is related to the tube growth rate dL/dt:

$$\frac{dV}{dt} \approx \pi R_T^2 \frac{dL}{dt}. \tag{10}$$

Substituting Eq. (10) into Eq. (9) gives

$$T \approx P_c\left[\frac{1.6R_B^4}{E\tau}\right]\frac{1}{\pi R_T^2}\frac{1}{dL/dt}. \tag{11}$$

This equation provides a testable relationship between observable quantities of the system.

In our current observations we have directly measured R_B, the individual T's, and the average values for R_T and dL/dt. At present, P_c has only been observed indirectly in the bowing of the structure. The linear relationship between the period and the pressure amplitude in Eq. (11) is in agreement with the data shown in Fig. 9. It should be possible to measure the pressure amplitude P_c directly by placing a pressure transducer into the fluid. This would then provide a measure of $E\tau$, the system's average Young's modulus times membrane thickness. Also, the base size R_B could easily be varied by varying the size of the initial pellet. This would provide another way of testing this relationship.

C. Model of osmosis and growth

When the pellet is first placed in the solution, it quickly dissolves, forming a concentrated solution of $Ca(NO_3)_2$ surrounded by membrane. $Ca(NO_3)_2$ is very soluble in water—a saturated solution has a molar concentration of 5 M. In aqueous solution there are three ions per mole, so this corresponds to a maximum interior osmotic pressure of approximately

$$P_{in} \approx \Re T 3 c_{in} \leq 360 \text{ atm}, \tag{12}$$

where $\Re$ is the ideal gas constant, T is the temperature, and c_{in} is the molar concentration. The inequality (12) is used because the interior solution is not always fully saturated. The exterior solution is 1 M sodium trisilicate ($Na_2Si_3O_7$) for which there are at most five ions per mole produced in aqueous solution, which corresponds to an exterior osmotic pressure of

$$P_{ex} \leq \Re T 5 c_{ex} = 120 \text{ atm}, \tag{13}$$

where c_{ex} is the exterior molar concentration. The inequality (13) is there because silica tends to produce aggregates in solution and so does not fully ionize. From these values it is clear that, as the pellet dissolves, the interior osmotic pressure will eventually become larger than the exterior; osmosis will drive water through the membrane and into the structure, causing it to grow.

The rate that water flows through the membrane is proportional to the pressure difference across the membrane. Because the typical osmotic pressures in Eqs. (12) and (13) are so much larger than the expected hydrostatic pressure differences that occur in the relaxation oscillation, the hydrostatic pressure differences can be neglected here. Thus the approximate volume flow rate into the structure from osmosis can be written as

$$\frac{dV}{dt} \approx \kappa \int dA[P_{in} - P_{ex}]. \tag{14}$$

Here the integral is over the surface of the structure and κ is a rate constant. Now, in principle, the surface of the structure is time dependent, while P_{in} and P_{ex} may also vary with position and time. However, the quantity of exterior liquid is much larger than that of the pellet, so it is reasonable to take the external concentration (and related osmotic pressure) to be a constant, independent of position or time. The interior concentration will generally not be a constant because dissolution of the pellet will increase the concentration while the osmotic flow of water into the structure and the loss of solute to form the membrane decreases the concentration. Using Eq. (12) we can rewrite Eq. (14) as

$$\frac{dV}{dt} \approx \mu \int_{S(t)} dA[c_{in}(\mathbf{r},t) - c_{in}^*], \tag{15}$$

where $\mu = 3\kappa\Re T$ and c_{in}^* is the interior concentration when the osmotic pressures balance. The position and time dependence in Eq. (15) has been shown explicitly.

Water stops flowing across the membrane, and the structure stops growing, $dV/dt = 0$, when the osmotic pressures balance. Thus the steady-state interior concentration c_{in}^* is an important quantity. It can be estimated using Eqs. (12) and (13) as

$$c_{in}^* \leq \frac{5}{3} c_{ex} = 1.7 \ \ M. \tag{16}$$

At this value the density of the interior solution is 1.19 g/ml. This should be compared to the density of the exterior solution, 1.06 g/ml. Thus, neglecting the membrane, the buoyant force on a tube will be downward. This agrees with our observation that the tubes do not always grow upwards in the current structure. The initial vertical growth of most tubes is probably caused by small bubbles inside the tube that are visible in the video recordings. A direct measurement of c_{in}^* should be possible and would be a useful result from future experiments.

The tube growth rate is proportional to the flow rate through the membrane, as described in Eq. (10). To gain some understanding of the average growth rate of the tubes, we will evaluate Eq. (15) under some crude, simplifying assumptions. First, we assume that the membrane is uniform. Although our previous discussion of stresses in the membrane indicated that the tube end must be different than the rest of the tube, this is a presumably a relatively small area and we will neglect this in the integration over the entire surface. Second, we assume that the interior concentration is uniform throughout the structure. We assume this because the pulsing nature of the fluid flow promotes mixing. Third, we assume that, on average, the tube has a uniform radius R. And finally, we assume that the pellet is fully dissolved before the first tube starts to grow. This last assumption is too simplistic at the start, when the pellet may not be fully dissolved, but should adequately describe the long-term behavior. All of these assumptions are rather crude, but our goal here is to produce the simplest possible model for describing the growth of the structure. More complicated models can be developed later as required by the data.

Using the stated assumptions, Eqs. (10) and (15) can be used to write the average tube growth rate as

$$\frac{dL}{dt} \approx \mu \frac{A(t)}{\pi R^2} \left[(c_0 + c_F) \left(\frac{V_B}{V(t)} \right) - (c_{in}^* + c_F) \right]. \tag{17}$$

Here all of the time dependence is in the surface area, $A(t)$, and the volume, $V(t)$, of the structure. These quantities are given by

$$A(t) = A_B + 2\pi R L(t),$$

$$V(t) = V_B + \pi R^2 L(t), \tag{18}$$

where the contributions of the base and tube have been separated. The quantity c_0 is the concentration in the base when $L=0$; it can be written as

$$c_0 = \frac{N - \phi A_B}{V_B}, \tag{19}$$

where N is the total number of moles of calcium nitrate in the pellet and ϕ is the number of moles per unit area of calcium nitrate in the membrane. The quantity c_F is defined as

$$c_F = \phi \frac{2}{R} \tag{20}$$

and is a constant related to the rate of solute loss to form the membrane of the tube. In general, since in this model all of the time dependence enters through the area and the volume of the structure, the behavior of the tube growth rate is dictated by the geometry of the structure. However, note that, while the observed structures typically have multiple tubes, our assumption of uniform concentration means that our model is insensitive to how the tubes are arranged. Thus Eqs. (17) and (18) provide a crude model for the growth of the total length of all the tubes on the structure, $L(t)$.

Initially, the interior concentration is large, so the growth rate given by Eq. (17) depends approximately on the ratio $A(t)/V(t)$. For a purely linear structure, $A(t)$ and $V(t)$ would both be proportional to $L(t)$, so the length and time dependences would cancel out. Thus the model predicts that the growth rate is relatively constant for most of the tube's growth. Because the structure is not purely linear, the growth rate actually increases initially (because the area grows faster than the volume) until the tube has the length

$$L_m \approx L_v \left(\sqrt{\frac{c_0 + c_F}{c^* + c_F}} - 1 \right), \tag{21}$$

where L_v is the length of the tube when the volume of the tube equals the volume of the base. After this point the growth rate decreases monotonically. Tube growth stops when the osmotic pressures balance. Setting $dL/dt = 0$ and solving for the tube length yields

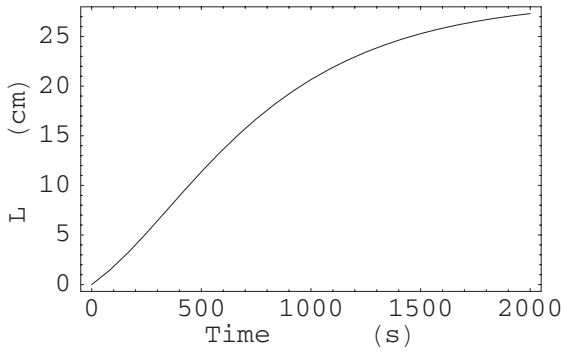

FIG. 12. The predicted tube length versus time. The model assumes the interior concentration is uniform throughout the structure and that the membrane thickness and the tube radius are also uniform. The initial time $t=0$ is when the first tube starts to grow (not when the pellet is first placed in the liquid).

$$L^* = L_v\left(\frac{c_0 - c^*}{c^* + c_F}\right). \tag{22}$$

This equation for L^* is relatively model independent; it just follows from conservation of solute. Note that both Eqs. (21) and (22) are finite even when the concentration of the exterior solution, c^*, goes to zero. In that limit, all of the interior solute goes into the membrane and none is left in the solution when growth stops.

To illustrate the tube growth predicted by this model, Fig. 12 shows the numerical solution of Eqs. (17) and (18). The total tube length versus time predicted by the model is plotted. Here we have taken the base to be a hemisphere with a radius of 0.5 cm and the average tube radius to be 0.075 cm, which corresponds to the dimensions shown in Fig. 1. The initial concentration is taken to be $c_0=5\ M$, the saturated concentration. The quantities c^* and c_f enter the model together; unfortunately, neither quantity has been measured directly. Lacking any better information, we have taken c^* to be the estimate in Eq. (16), while c_F was taken to be zero. With these parameters the model predicts the growth rate to be relatively constant, with a slight peak at $L_m=7.6$ cm and a total tube length of $L^*=29$ cm. While L_m was not able to be measured accurately because of the twisting of the tube, the predicted total tube length L^* is compatible with what is observed. The rate constant was obtained by setting the maximum growth rate in the model to the maximum growth rate given in Fig. 11, to yield $\mu=5.0\times10^{-2}$ cm^4/mol s. In general, the behavior shown in Fig. 12 agrees well with the current observations.

Independent of the model, a decreasing interior concentration may affect how the membrane forms at the end of the tube. Lower concentrations may cause the membrane to form more slowly. This would decrease the average critical pressure P_c [see Eq. (11)]. However, since solute loss and inflow dilution are both largest at the ends of the tube, it is to be expected that these regions will reach the steady-state concentration c_{in}^* before the rest of the structure. Thus it is probable that the average critical pressure is also in steady state for much of the later tube growth. Direct observation of the critical pressure may be possible in the future by placing a transducer into the exterior fluid. This would give some additional information on the change in concentration in the structure.

D. Model of the relaxation oscillations

In the previous section we described how the structure changes on relatively long time scales. Here we examine how the structure changes on short time scales, the time scales of the relaxation oscillation. The dynamical processes occurring at the tube end are the key to the relaxation oscillations. In order to understand these processes better, we discuss here a simple model of how things change in time at the tube end. Our goal is to understand why the oscillations occur and what determines the period of the oscillations and the radius of the tube.

At the hemispherical tube end (with radius R), the change in stress with time is given by differentiating Eq. (1):

$$\frac{d\sigma_{tube\ end}}{dt} = \frac{R}{2\tau}\left[\frac{dP}{dt} - \frac{P}{\tau}\frac{d\tau}{dt}\right], \tag{23}$$

where t is time. The first term describes the increase in stress from the buildup in internal pressure while the second term describes the decrease in stress from the growth in thickness of the membrane. The rate of pressure increase, dP/dt, depends on the global properties of the structure and can be taken as a constant over a relaxation oscillation (see Secs. IV B and IV C). The rate of membrane growth is unknown, but given that we are interested in the growth only over a time short compared to the time to reach its steady-state value, a reasonable first guess is to model these processes as scale free—i.e., a power law:

$$\frac{d\tau}{dt} \approx \frac{\alpha}{\tau^\gamma}, \tag{24}$$

where α is a constant and γ is the scaling exponent. This form is also suggested by another consideration. Since membrane growth occurs from solute diffusing through the membrane, Fick's first law of diffusion would suggest the form in Eq. (24) with $\gamma\approx1$.

To describe what happens during one oscillation cycle, we solve Eq. (24) and substitute this into Eq. (23). Then

$$\frac{d\sigma_{tube\ end}}{dt} = \left[\frac{\gamma}{1+\gamma}\right]\left(\frac{R}{2\tau}\right)\left(\frac{dP}{dt}\right). \tag{25}$$

The only time-dependent quantity on the right-hand side of Eq. (25) is the tube thickness τ, which grows monotonically with time. Thus in this simple model the stress at the tube end starts at zero, then grows monotonically until it reaches the critical value, σ_c, at which point the membrane ruptures. Note that $\gamma>0$; otherwise, the stress would decrease in time and the membrane would never rupture. Equation (25) can be integrated to give an expression for the period of the oscillation:

$$T = A\left[\frac{1}{R^{1+1/\gamma}}\right],$$

$$A = [\alpha(\gamma+1)]^{1/\gamma}\left[\frac{2\sigma_c}{(dP/dt)}\right]^{1+1/\gamma}. \quad (26)$$

Thus in this model the period is determined by membrane properties (α, γ, and σ_c), the rate of pressure increase (dP/dt), and the radius of curvature at the tube end (R).

Tubes are not smooth, but instead are observed to fluctuate in radius and direction. The tube radius is determined dynamically by the processes that occur at the end of the tube: membrane rupture, liquid emergence, and new membrane growth. In general, it is common for membrane rupture to have a stochastic distribution around an average value (see, e.g., [17]). This fact and Eq. (26) provide an explanation for the observed fluctuations in the period, Figs. 6 and 7. To model these process quantitatively, we look for a map that describes how the tube radius during one cycle arises from the tube radius of the previous cycle:

$$R_{n+1} = f(R_n) + \xi_n. \quad (27)$$

Here R_n is the radius of the tube end before the nth rupture and ξ_n is a variable parametrizing the stochastic fluctuations in the rupture process. The function f in Eq. (27) describes how the dynamics responds to the previous fluctuations.

How the curvature of the tube end changes from rupture and liquid emergence is predominantly a geometry problem, so we hope to gain insight into the function f by considering the relevant macroscopic length scales. Their are only two, one is the present radius of the tube end, R_n, and the other is the length associated with the amount of interior liquid that emerges at the time of the nth rupture:

$$\rho_n = c\left(\frac{dV}{dt}T_n\right)^{1/3}, \quad (28)$$

where T_n is the time interval that the tube has radius R_n and c is a dimensionless geometric factor. We will use dimensional analysis and write f as a combination of the two length scales R_n and ρ_n.

Further insight into the nature of the function f can be obtained by considering how much the tube grows in each cycle. With each cycle the tube grows on average by an amount ΔL:

$$\Delta L = \frac{dL}{dt}T \approx 0.2 \text{ mm}, \quad (29)$$

where we have used the observed average values for the tube growth rate and the period. Comparing this to the typical radii, 0.5–1 mm, we find

$$\frac{R}{\Delta L} \approx 3-6. \quad (30)$$

Thus it takes several oscillations for the tube to grow a length equal to its radius. Because the tube length grows so little with each rupture, the average tube radius cannot change very much with each rupture. Thus the function f is approximately the old tube radius plus a small correction. For the small correction, is should be reasonable to use a linear approximation. Combining all of this information on the function f, we choose to approximate it as

$$f \approx R_n + \beta(\rho_n - R_n), \quad (31)$$

where β is a dimensionless parameter. Combining Eqs. (26)–(28) and (31) gives

$$R_{n+1} = (1-\beta)R_n + \beta c\left[\frac{dV}{dt}A\right]^{1/3}\left[\frac{1}{R_n}\right]^{\gamma+1/3\gamma} + \xi_n. \quad (32)$$

This is the equation we shall use to model how one cycle relates to the next.

Expanding Eq. (32) about the fixed point R^*, the map can be approximated as $R_{n+1}-R^* \approx \lambda(R_n-R^*)$. The multiplier λ that describes the approach to the fixed point is given by

$$\lambda = 1 - \frac{\beta}{3}\left(4+\frac{1}{\gamma}\right). \quad (33)$$

This is the multiplier not just for the radius, but also for the period, since the period is just a function of the radius. The fixed point is stable when the multiplier has a magnitude less than 1. This corresponds to the range of β values

$$0 < \beta < \frac{6}{4+\frac{1}{\gamma}}. \quad (34)$$

The value of λ can be obtained directly from the autocorrelation of the period data, as presented in Fig. 8. In these figures, λ is just the ratio of the nth point over the $(n-1)$th point, until n gets large and the stochastic fluctuations destroy the correlation. Using the $n=1$ point of the two data sets gives

$$\lambda \approx 0.24. \quad (35)$$

Note that Eq. (33) is relatively insensitive to the value of γ since $\gamma>0$, and so β can estimated from the experimental data:

$$\beta \approx \begin{cases} 0.46, & \gamma = 1, \\ 0.57, & \gamma = \infty. \end{cases} \quad (36)$$

Going back to Eq. (31), we note that this value of β has a simple, physical interpretation. The new radius R_{n+1} is approximately just the mean of the two relevant length scales R_n and ρ_n.

To extract c from the observations, we note that the fixed point of Eq. (31) is when

$$\rho = R. \quad (37)$$

Using Eqs. (10), (28), and (30) and solving for c gives

$$c = \left[\frac{R^*}{\pi\Delta L}\right]^{1/3} \approx 1.0-1.2. \quad (38)$$

Using these values for c, we can use our model to make predictions for the period and the radius of the tubes under different situations.

Solving Eq. (32) for the fixed point radius gives

$$R^* = \left\{\alpha(\gamma+1)c^{3\gamma}\left[2\sigma_c\frac{V}{B}\right]^{\gamma+1}\left[\frac{dV}{dt}\right]^{-1}\right\}^{1/4\gamma+1}. \quad (39)$$

Here B/V is the bulk modulus of the system divided by the volume of the system (see Sec. IV B). Note that this equation

is independent of β. Since the period is a function of R, we can substitute this into Eq. (26) and get an expression for the fixed point value of the period:

$$T^* = \left\{ \alpha(\gamma+1)\left[\left(\frac{2\sigma_c}{c}\right)\left(\frac{V}{B}\right)\left(\frac{dV}{dt}\right)^{-4/3}\right]^{\gamma+1}\right\}^{3/4\gamma+1}. \quad (40)$$

These equations give the value of the radius and the period in terms of fundamental parameters of the system. Unfortunately, there are more fundamental membrane parameters in Eqs. (39) and (40) then we cannot solve for with the present data.

Aside from fundamental parameters dealing with the membrane properties (α, γ, and σ_c) the fixed point depends on the pressure response of the system (B/V) and the rate of flow of liquid into the structure (dV/dt). As discussed in Sec. IV B, the pressure response of the system is dominated by membrane around the base and so is expected to be a constant as tubes grow from the base structure. Also, as discussed in Sec. IV C, the flow rate is proportional to the tube growth rate (dV/dt) which is observed to be a constant over most of the structures growth. Thus our model predicts that the average radius and period should also be constants over most of the structures growth. This agrees with our observations.

Experiments have been performed in Refs. [11–13] where tubes have been grown, not from a pellet, but from direct injection of metal salt solution into an exterior silicate solution. This technique has the advantage of allowing the flow rate to be controlled. Our model predicts that the tube radius scales with the flow rate as

$$R^* \propto \left[\frac{dV}{dt}\right]^{-1/4\gamma+1} = \begin{cases} \left[\frac{dV}{dt}\right]^{-0.2}, & \gamma = 1, \\ 1, & \gamma = \infty. \end{cases} \quad (41)$$

Similarly, the period scales as

$$T^* \propto \left[\frac{dV}{dt}\right]^{-4(\gamma+1)/4\gamma+1} = \begin{cases} \left[\frac{dV}{dt}\right]^{-1.6}, & \gamma = 1, \\ \left[\frac{dV}{dt}\right]^{-1}, & \gamma = \infty. \end{cases} \quad (42)$$

Note that these scaling equations are relatively insensitive to the value of γ, the parameter which describes how the membrane grows. Equation (41) indicates that the radius is essentially constant, independent of the flow rate, while Eq. (42) indicates that the period varies inversely with the flow rate.

These model predictions can be compared with the results in Refs. [11,12]. In Ref. [11] they measured the period and the growth rate of cupric sulfate injected into silicate solution. When the tube was in "popping" mode, they found that the product of the flow rate and the period was essentially a constant. This in agreement with Eq. (42), especially for a value of γ somewhat larger than one. They also measured the growth rate and found that it was proportional to the flow rate. This implies that the tube radius is constant, independent of the flow rate, in agreement with Eq. (41). However, in subsequent measurements, Ref. [12] found the radius to grow slightly at higher flow rates. It must be emphasized that caution should be used when comparing our model to the results of Refs. [11–13] which use an injection method. For one thing, their "popping" mode can sometimes give a droplet that disengages from the tube, qualitatively different than the mode analyzed herein. More importantly, our analysis clearly indicates that the pressure response of the system is important for the relaxation oscillations. We have assumed in Eqs. (41) and (42) that the pressure response of the system, B/V, is a constant as it is for the pellet system (see Sec. IV B) where it is dominated by the base structure. However, for the injection method, there is no base structure and it is not clear what controls the pressure response of their system.

One future experiment that should be straightforward to perform is to measure how the growth of the structure changes with the size of the initial pellet. Following the discussion of Sec. IV C, we shall assume that dV/dt scales approximately as the square of the base radius. Similarly, in Sec. IV B we analyzed the pressure response of the system, B/V, and found that it scales as one over the base radius to the fourth power. Then Eqs. (40) and (39) predict that the tube radius scales with the base radius R_B as

$$R^* \propto R_B^{4\gamma+2/4\gamma+1} = \begin{cases} R_B^{1.2}, & \gamma = 1, \\ R_B, & \gamma = \infty. \end{cases} \quad (43)$$

Similarly, the period scales with the base radius as

$$T^* \propto R_B^{4(\gamma+1)/4\gamma+1} = \begin{cases} R_B^{1.6}, & \gamma = 1, \\ R_B, & \gamma = \infty. \end{cases} \quad (44)$$

Note that these scaling equations are again relatively insensitive to the value of γ, the parameter which describes how the membrane grows. Thus we can still make some predictions even though the value of γ is unknown.

V. SUMMARY AND FUTURE WORK

Here we have reported data from videotaping the growth of treelike chemical garden structures (Fig. 1). The videotapes show something that has never been observed before, a chemical garden structure that undergoes regular motion—a slow bowing downward of the "branches" followed by a quick twitch upwards (Fig. 4). The motion is a side effect of the relaxation oscillation whereby the structure grows. Osmosis drives water into the structure, increasing the internal pressure and causing the structure to visibly "bow" or "flex" (Fig. 3). When the internal pressure gets too great, the membrane ruptures and internal fluid emerges (Fig. 5). The release of the internal pressure allows the structure to quickly relax to its unbowed state. Membrane quickly forms around the extruded fluid, extending the structure. Long, tubular arms grow from a series of several hundred of these rupture and healing cycles.

The videotape data provide details on how the chemical gardens grow. The average growth rate of the tubes has been measured at different times and found to be relatively constant for most of the structures growth (Fig. 11). The period of the oscillations is much easier to measure, and it is observed that the average period also is also relatively constant,

increasing somewhat at late times (Figs. 10). From cycle to cycle, the period fluctuates a considerable amount (Figs. 6 and 7). This is typical for a quantity sensitive to a rupture process. The fluctuations are relatively stochastic, with little if any correlation more than a few intervals apart (Fig. 8). However, there is typically a strong correlation between the amplitude of the observed motion and the length of the preceding time interval (Fig. 9). This is easily understandable: the longer for the pressure to build up the larger the subsequent relaxing motion of the structure.

Our analysis of stresses in the membrane tells us some interesting facts about the membrane rupture and growth. That the membrane consistently ruptures at the tube end tells us that the young membrane there is more than 5–10 times weaker than old membrane [Eq. (3)]. That is, the membrane must strengthen on a time scale that is much longer than the oscillation period. Following the stress calculations with a study of the corresponding strains, we have calculated the change in volume of the structure from a pressure increase. This calculation provides a relationship between several observable quantities: the period and amplitude of the oscillations, the average growth rate, and the average radii of the base and the tube [Eq. (11)]. This relationship predicts that the period of the relaxation oscillation should be linearly proportional to the amplitude, in agreement with observations. It also relates how the averages of these quantities change on longer time scales, which may be observable in future experiments.

Osmosis drives water through the membrane into the structure, causing it to grow. We have constructed a crude model for the long time scale growth of the structure—i.e., the growth averaged over the oscillations [Eqs. (17) and (18)]. As the structure grows, the membrane surface area increases which increases the flow rate. However, what also happens as the structure grows is that the internal fluid becomes more dilute, from water inflow and from loss of solute to membrane construction, which decreases the osmotic flow. These two effects balance out for most of the structures growth, resulting in a relatively constant growth rate (Fig. 12). This is in agreement with our observations (Fig. 11).

We have also constructed a model of the short-time-scale behavior of the system—i.e., the relaxation oscillations. Our model focuses on two quantities: the period of the oscillations and the radius of curvature of the tube end. These two quantities are related in two different ways. Considering the membrane stress at the tube end, the smaller the radius of curvature at the tube end the smaller the stress so the longer the time it takes to reach the membrane's critical stress. Thus membrane stress considerations imply that the period varies approximately inversely with the radius, Eq. (26). Another relation between the period and the tube end radius arises from the geometry of tube formation. The longer the period, the more fluid that flows into the structure from osmosis and so the more fluid extruded through the tube end when rupture occurs. Assuming the volume of the tube end is proportional to the volume of fluid emitted, Eq. (37), provides us with another relationship between the period and the tube end radius—i.e., that the period is proportional to the cube of the tube end radius. These two relations can be solve to yield expressions for the average tube radius and the average period in terms of fundamental membrane parameters: the flow rate and the pressure response of the system [Eqs. (39) and (40)]. While the fundamental membrane parameters are currently unknown, we have used the model to predict how the average radius and period scale with the size of the pellet and with the flow rate [Eqs. (41)–(44)]. These scaling relations are relatively insensitive to the unknown membrane parameters.

Our model for the relaxation oscillations is expressed in the form of a one-dimensional map. The map parametrizes how the tube end radius of one cycle arises from the radius of the previous cycle. Fitting the map to the autocorrelation data (Fig. 8), the data imply that the new radius is the mean of the old radius and the length scale associated with the emitted fluid, Eq. (36), plus stochastic fluctuations.

Our analysis has suggested many areas for future experimental exploration. Varying the size of the initial pellet is a straightforward way to test our model of the relaxation oscillations. Two other measurements that would be useful are the amount of solute per area in the membrane and the steady-state interior concentration. These measurements would improve the model of tube growth. Also, direct measurement of the elasticity of the membrane would eliminate the unknown constants in the bulk modulus. Another useful observation would be the simultaneous measurement of tube length and motion. In our present observations, tube growth was only measured for the initial growth of a tube when the tube was straight and the oscillation movement too small to observe. Simultaneous measurement of length and motion over extended periods of time would check Eq. (11).

One of the most interesting possible observations would be a direct measurement of the pressure changes in the fluid. The membrane ruptures should cause a pressure wave in the fluid that may be detectable directly by placing a hydrophone into the solution. Such measurements would provide some information on the nature of the rupture process that occurs at the tube end. More importantly, they would provide a measure of the relaxation oscillations completely independent of the videotape analysis. Such measurements could help sort out the reasons for the motion—i.e., how much comes from asymmetric stresses and how much from buoyancy changes. Also, knowledge of how the pressure amplitude changed in time would give information on how the growth of the membrane at the tube end changed in time.

Another interesting experiment would be to see how the relaxation oscillation responded to pressure pulses from a transducer. It should be possible to induce a rupture at the tube end with such a pressure pulse. In that case, one could synchronize the relaxation oscillation to these pressure pulses. This would give some control over the growth of the tube.

ACKNOWLEDGMENT

This work was supported in part by National Science Foundation Grant No. CHEM 0608631.

[1] J. R. Glauber, *Furni Novi Philosophici* (Amsterdam, 1646).
[2] S. Leduc, *The Mechanism of Life* (Rebman, London, 1911); A. L. Herrera, *Boletin de la Direccion de Estudios Biologicos, Mexico* (Instituto Medico Nacional, Mexico, 1916–1917), Vols. 1–2.
[3] D. D. Double and A. Hellawell, Nature (London) **261**, 486 (1976); D. D. Double, A. Hellawell, and S. J. Perry, Proc. R. Soc. London, Ser. A **359**, 435 (1978); J. D. Birchall, A. J. Howard, and J. E. Bailey, *ibid.* **360**, 445 (1978); D. D. Double, P. C. Hewlett, K. S. W. Sing, and J. F. Raffle, Philos. Trans. R. Soc. London, Ser. A **310**, 53 (1983).
[4] A commercial chemical garden kit is marketed under the name "Magic Rocks" and can by purchased at many toy stores.
[5] D. E. H. Jones, Am. Sci. **90**, 454 (2002).
[6] P. R. D. Coatman, N. L. Thomas, and D. D. Double, J. Mater. Sci. **15**, 2017 (1980); J. Maselko, A. Geldebhuys, J. Miller, and D. Atwood, Chem. Phys. Lett. **373**, 563 (2003); J. Maselko, P. Borisova, M. Carnaham, E. Dreyer, R. Devon, M. Schmoll, and D. Douthat, J. Mater. Sci. **40**, 4671 (2005).
[7] S. Thouvenel-Romans, J. J. Pagano, and O. Steinbock, Phys. Chem. Chem. Phys. **7**, 2610 (2005); D. A. Stone and R. E. Goldstein, Proc. Natl. Acad. Sci. U.S.A. **101**, 11537 (2004).
[8] J. H. E. Cartwright, J. M. Garcia-Ruiz, M. L. Novella, and F. Otalora, J. Colloid Interface Sci. **256**, 351 (2002).
[9] T. S. Sorensen, J. Colloid Interface Sci. **79**, 192 (1981).
[10] T. H. Hazlehurst, J. Chem. Educ. **18**, 286 (1941).
[11] S. Thouvenel-Romans and O. Steinbock, J. Am. Chem. Soc. **125**, 4338 (2003).
[12] S. Thouvenel-Romans, W. van Saarloos, and O. Steinbock, Europhys. Lett. **67**, 42 (2004).
[13] J. J. Pagano, T. Banasagi, Jr., and O. Steinbock, J. Phys. Chem. C **111**, 9324 (2007).
[14] A. Costa, O. Melnik, R. S. J. Sparks, and B. Voight, Geophys. Res. Lett. **34**, L02303 (2007).
[15] J. Davidsen, S. Stanchits, and G. Dresen, Phys. Rev. Lett. **98**, 125502 (2007).
[16] J. F. Harvey, *Theory and Design of Modern Pressure Vessels* (Van Nostrand Reinhold, New York, 1974).
[17] E. Evans, V. Heinrich, F. Ludwig, and W. Rawicz, Biophys. J. **85**, 2342 (2003).